RSC Advances

This article can be cited before page numbers have been issued, to do this please use: Y. Peng, G. Jing and T. Cui, *RSC Adv.*, 2015, DOI: 10.1039/C5RA19343E.

ROYAL SOCIETY OF CHEMISTRY

www.rsc.org/advances

View Article Online
DOI: 10.1039/C5RA19343E

Journal Name

ARTICLE

High Performance Perovskite Solar Cells through Vapor Deposition with Optimized PbI_2 Precursor Films

Received 00th January 20xx,
Accepted 00th January 20xx

DOI: 10.1039/x0xx00000x

www.rsc.org/

Yanke Peng[a†], Gaoshan Jing[a†] and Tianhong Cui*[ab]

Quality of a perovskite film would determine the performance of a perovskite solar cell. A novel hybrid physical-chemical vapor deposition (HPCVD) method is presented to grow high quality $CH_3NH_3PbI_3$ films. These films were synthesized in a vacuum quartz tube with a constant growth temperature of 100 °C, resulting in the uniform film with grain sizes up to 800 nm and surface roughness about RMS 17.4 nm. Combined with optimized spin coating process for PbI_2 precursor films, a high-performance $CH_3NH_3PbI_3$ solar cell's power conversion efficiency (PCE) can reach up to 14.2%. When treated in a controlled harsh environment at 80 °C for 96 hours, ten solar cells still maintained 78% of their initial efficiency averagely, which demonstrates effectiveness of this HPCVD method.

Introduction

Hybrid inorganic and organic perovskite materials have shown tremendous potentials for photovoltaic research and development in recent years [1, 2]. Since the first perovskite solar cell was introduced in 2009, its power conversion efficiency (PCE) has jumped from 3.8% [3] to 20.1% [4] in five years, unprecedented in the history of photovoltaics (PV). In the meantime, more mature silicon-based PV researches have shifted to design and construct nanostructures on solar cell surfaces to collect light more efficiently through concentration and trapping [5-7]. A typical perovskite solar cell (e.g., $CH_3NH_3PbI_3$) can be prepared by simple solution based methods with such advantages as high power conversion efficiency, low material and fabrication cost [8-11]. Due to superior properties of perovskite materials as optical absorption layers for a solar cell, such as appropriate direct band gap [12], high absorption length for visible light spectrum [2], long carrier diffusion length and intrinsically low defect levels [13-15], perovskite solar cells become the most competitive research in photovoltaics in recent years. Crystalline quality of a perovskite film, including perovskite crystalline grains and the uniformity of morphology, would greatly determine the performance of perovskite solar cells [11, 16-18]. In addition, optical [19, 20], electrical [21-24] and semiconductor properties [13, 14, 25, 26] of perovskite materials are highly determined by synthesize methods. For broad applications of perovskite solar cells in the future, it is necessary to develop methods to synthesis high-quality, uniform, and stable perovskite film at a large scale.

Hybrid perovskite was synthesized by chemical reaction of two precursors, lead halide (e.g., PbI_2) and methylammonium halide (e.g., CH_3NH_3I). Up to now, solution based and vapor based method are the two most popular methods utlized to sysnthesize perovskite films. The solution based method for perovskite solar cells included one-step and two-step deposition methods. In one-step deposition method [8], lead halide (e.g., PbI_2) and methylammonium halide (e.g., CH_3NH_3I) were mixed in an organic solvent, such as N, N-dimethylformamide (DMF), N-methyl-2-pyrrolidone γ-butyrolactone (GBL), or dimethylsulphoxide (DMSO), followed by a spin-coating of the mixture solution and a baking on a substrate to form a perovskite thin film. Meanwhile, perovskite thin films can also be prepared by two-step deposition [9]. One major challenge of solution-based methods is that materials making perovskite in solution crystallize too fast to form a uniform perovskite film due to the uncontrollable and slow evaporation speed of perovskite solvent [11]. Recently, various procedures have been demonstrated to improve the crystallization process for solution based methods: (1) dripping toluene when the perovskite solution was spin-coated [11] and (2) adding argon flow when the solution was spin-coated onto the substrate to increase the solvent evaporation process to acquire perovskite films with smooth surface, uniform thickness, and large grain size [27, 28]. Additionally, post thermal annealing the perovskite films after spin coating in ambient air with 30%±5% relative humidity, was introduced to enhance the re-crystallization effect for forming uniform films and reducing the boundary defects between perovskite grains [17, 29]. Nonetheless, it is still technically demanding to synthesize uniform perovskite film of high quality with small surface roughness using solution-based methods.

[a] State Key Laboratory of Precision Measurement Technology and Instruments, Department of Precision Instruments, Tsinghua University, Beijing, 100084, China
[b] Department of Mechanical Engineering, University of Minnesota, Minneapolis, Minnesota 55455, USA. Phone: 001-612-626-1636 Email: tcui@me.umn.edu
† The first two authors contributed equally to this work.
Electronic Supplementary Information (ESI) available: [Additional experimental introduction and data].

View Article Online
DOI: 10.1039/C5RA19343E

Several vapor based methods were also developed to grow high-quality perovskite film, including dual source co-evaporation [16, 30], vapor assistant solution deposition [18], and hybrid chemical vapor deposition (CVD) [31-34]. In dual source co-evaporation, methylammonium halide and lead halide precursors were evaporated at 120 °C and 325 °C simultaneously in an ultra high vacuum chamber and reacted on a fluorine doped tin oxide (FTO) glass substrate to fabricate a solar cell with 15.4% efficiency [16]. In vapor assistant solution deposition process (VASP), a layer of PbI_2 film was formed by spin coating firstly, and then reacted with methylammonium halide (e.g., CH_3NH_3I) vapor in a glove box to generate a uniform perovskite film. A solar cell of 12.1% efficiency was achieved with VASP pervoskite films, crystalline grain sizes and surface roughness of which were about 500 nm and RMS 23.2 nm, respectively [18]. By a chemical vapor deposition method, single crystalline perovskite nanoplateles were grown on a muscovite mica surface with an electron diffusion length greater than 200 nm [31]. Another vapor based method using low-pressure chemical vapor deposition (LPCVD) was applied to synthesize perovskite film, which was utilized to make a solar cell with a efficiency of 12.74% [34]. However, vapor based methods are not widely used to synthesize high quality perovskite thin films due to the complexity and challenge to control chemical and physical reactiones in vapor phase. Perovskite films synthesized by dual sources co-evaporation needed to deal with two solid precursors at two different melting temperatures: one is lead halide with a melting temperature at 325 °C, and the other is methylammonium halide with melting temperature at 125 °C. From previous research findings, perovskite thin film would degenerate over 145 °C [35]. Therefore, traditional evaporation and CVD process would not be appropriate to synthesize perovskite films without optimizing the conventional CVD system and deposition process. Meanwhile, critical parameters for vapor reaction process, for instance reaction temperature and vapor pressure, could not be optimized for these vapor based processes to make high quality perovskite materials.

In this letter, we introduce a novel HPCVD method to synthesize high-quality perovskite films of $CH_3NH_3PbI_3$ for fabricating high-performance solar cells. Comparing to existing solution and vapor based methods, $CH_3NH_3PbI_3$ films would be synthesized in a vacuum and isothermal environment through uniform gas phase and solid phase reaction. In our previous work, several parameters for HPCVD method have been discussed to optimize the perovskite film synthesizing, such as reaction temperature [36] and vapor pressure [37]. With a high quality PbI_2 precursor film by optimized spin coating process, quality of $CH_3NH_3PbI_3$ thin films could be further improved. The reaction temperature of 100 °C is one of the lowest synthesizing temperatures for $CH_3NH_3PbI_3$ material, as far as we know. In ambient environment, PbI_2 solid thin films were fabricated by an optimized solution based spin coating process on a mesoporous TiO_2 (m-TiO_2)/compact TiO_2 (c-TiO_2)/FTO substrate. Next, purified CH_3NH_3I crystal solid precursor was laid into a quartz boat, which would loaded into an isothermal vacuum quartz tube, and the evaporated CH_3NH_3I vapor would react with the solid PbI_2 film to form a uniform $CH_3NH_3PbI_3$ thin film. However, a different reported CVD method [31] to synthesize perovskite films utilized nitrogen flow to bring the CH_3NH_3I vapor evaporating from a high temperature zone (185 °C) to react with PbI_2 films at a relative low temperature zone (about 130 °C). In our method, vacuum of 2 mTorr and low constant temperature of 100 °C were maintained to reduce perovskite film growth rate and decrease perovskite film defects. High PCE of these solar cells up to 14.2% (reverse scanning) was achieved. After treated in a controlled harsh environment (80 °C for 96 hours), ten solar cells by HPCVD still maintained 78% of their initial efficiency (decreasing from 8.9% to 6.9%, averagely), which demonstrates the effectiveness of this new HPCVD method. The HPCVD method is comparable with tradional semiconductor material growth methods and high quality perovskite films could be synthesized under precise process controls. In future, high performance perovskite solar cell could have great potential to be produced on a large scale at low cost by HPCVD for various application scenarios.

Experimental

Substrate preparation

FTO transparent conductive glass (Tec15, Pilkington) was patterned by laser etching. The substrates were cleaned in deionize (DI) water, ethanol, aceton, and isopropyl alchohol (IPA) sequentially for 15 min by ultrasonication. Then, fifteen minutes oxygen plasma treatment was used to eliminate organic residues on surfaces of the substrates.

Solar cells fabrication

A 20~40-nm-thick compact TiO_2 layer was spin coated on the FTO substrat according to the previous paper [16]. Then, 200-nm-thick mesoporous TiO_2 layer was spin coated onto the sintered comparct TiO_2 surface at 5000 rpm for 15 s using a commercial TiO_2 paste (NJU-SR, Sunlaite, Suzhou, China) diluted in ethanol with 20% weight ratio. The mesoporous TiO_2 films were formed after sintering at 500 °C for 30 min to remove organics in the paste. Then, the TiO_2 coated substrates were treated in a 50 mM $TiCl_4$ aqueous solution at 70 °C for 30 min. After cleaning with DI water and ethanol, the substrates were sintered again at 500 °C for 30 min. PbI_2/N, N-dimethylformamide (DMF, Sigma) solution (461 mg mL^{-1}) were prepared on a hotplate of 70 °C with stirring. PbI_2/DMF solution was maintained at 70 °C before spin coated on substrates to keep its viscosity at an optimized range. After heated at 70 °C for 30 min to thoroughly remove the DMF residue, the PbI_2 substrates were loaded into a quartz tube with CH_3NH_3I powder evenly spreaded below. After the tube was sealed with flanges and o-rings and vacuumized with a oil pump, 80 sccm nitrogen flow was purged into the tube last for 20 min, and the tube was heated simultaneously to 50 °C to remove residual water vapor and oxygen gas inside. Then, the nitrogen flow was cut-off and the quartz tube was pumped to a vaccuum level of 2 mTorr. The exact temperature in the

View Article Online
DOI: 10.1039/C5RA19343E

tube was 100 °C though the heating program of the quartz tube furnace was set at 110°C, which was calibrated by a wireless PT1000 temperature recorder (TP-1000-W1, A-Volt Co., Ltd, Beijing, China) placed inside the vacuum tube during the whole heating procedure (calibrated temperature curve shown in Figure S2). After the solid PbI_2 films and CH_3NH_3I gas reacted in the tube for three hours, the substrates with perovskite films were took out from the tube and annealed at 100 °C for 10 min at a relative humidity 30%±5% in ambient air. Then hole transport layers were formed by spin coating 150 nm spiro-OMeTAD (Lumtech, Taiwan) on top of the perovskite films following previous reported methods [9]. Finally, 60 nm gold films were deposited by E-beam evaporation as back electrodes at a spead of 0.3 anstrom per second. Dimension of the gold electrode pad was 4*4 mm.

Characterizations

Surface profiles of PbI_2 films, perovskite films and the cross-sectional of perovskite solar cell were measured by a field-emission scanning electron microscope (FE-SEM, Zeiss Merlin). Current density-voltage (*J-V*) curves of solar cells were characterized by a Semiconductor Device Parameter Analyzer (B1500A, Keysight, USA). The *J-V* curves were measured under AM 1.5 illumination (100 mW cm^{-2}) generated by a Newport ABB (94021A) solar simulator in ambient air. Light intensity of the solar simulator was calibrated by a Newport mono-silicon reference cell (Newport calibration cert. #0702). A 3*3 mm steel mask was covered on solar cells during the measurements. The voltage scan condition of *J-V* curves was 1.2V~-0.1V~1.2V with a 20 mV step and 50 ms delay. Also, Incident Photon to Current Conversion Efficiencies (IPCE) of the perovskite solar cells by HPCVD were measured in the wavelength from 300 to 900 nm (Oriel IQE 200, Newport, USA) at direct current (DC) mode.

Results and Discussions

High quality of the $CH_3NH_3PbI_3$ film could be attributed to the advantages of the HPCVD method, including controllable vacuum environment, isothermal growing conditions, as well as the optimization of making PbI_2 solid precursor film and isothermal process prior to and after the perovskite film synthesis.

Vacuum level and constant growing temperature are two critical parameters to achieve high-quality $CH_3NH_3PbI_3$ films. Typically, glove boxes filled with nitrogen were used to synthesize perovskite materials by solution methods to prevent solar cells degradation caused by high humidity and oxygen in ambient air [9]. For our method, the quartz tube was inlet 80 sccm nitrogen flow and pre-heated at 50 °C in order to remove probable water vapor and oxygen gas trapped inside these two precursor materials. After turning off the nitrogen flow, the quartz tube was pumped to 2 mTorr. Such vacuum level of the tube was maintained by running the pump consistently to avoid leakage contamination from the ambient environment. Two solid precursors (PbI_2 and CH_3NH_3I) were placed inside an isothermal region with a length of about 50 cm. Once the tube temperature was elevated to a constant temperature of 100 °C, CH_3NH_3I vapor was generated and reacted with the solid PbI_2 precursor thin films. High-quality $CH_3NH_3PbI_3$ films were achieved by this vacuum based isothermal process. Characterized by scanning electron microscopy (SEM), grain size of a $CH_3NH_3PbI_3$ film is average 300 nm while the largest grain size reaches over 800 nm, as shown in Figure 1a. Surface roughness of the $CH_3NH_3PbI_3$ film was measured by atomic

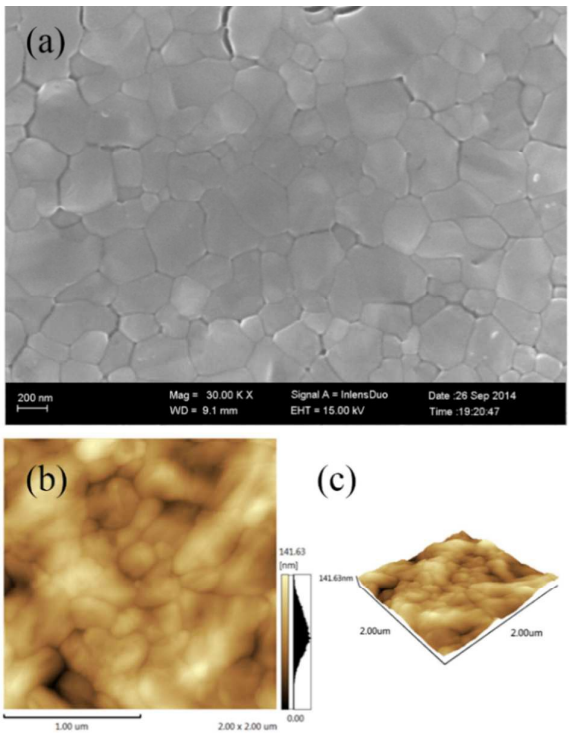

Fig. 1 A $CH_3NH_3PbI_3$ film on a FTO/c-TiO_2/m-TiO_2 substrate prepared by HPCVD method in a quartz tube at 100 °C for 3 h without thermal annealing: (a) a top view SEM image with a grain size about 300 nm; (b) tapping-mode AFM height image of the perovskite film with surface roughness about RMS 17.4 nm; (c) corresponding 3D AFM image.

force microscopy (AFM). A smooth $CH_3NH_3PbI_3$ was also obtained by this process with a surface roughness less than RMS 17.4 nm, as show in Figure 1b, significantly smaller than previous publication result [18]. Large gain sizes would decrease photo-generated carriers scattering during transporting inside the material. Low surface roughness would decrease carrier surface recombination when transporting between the interface of electron/hole transport layer and perovskite film.

Quality of the solid PbI_2 precursor films also determine resulting $CH_3NH_3PbI_3$ films. PbI_2 films were prepared by solution-based spin-coating process, and film thickness and uniformity were affected by rotating speed and vapor exhaustion condition, which would affect the recrystallization speed of PbI_2 material. As shown in Figure 2b, the uniformity of PbI_2 film is poor when spin-coating at 3000 rpm. By increasing rotating speed to 5000 rpm, the uniformity is greatly improved because of faster crystallization of PbI_2, as shown in Figure 2c. Higher spin coating speed would lead to

View Article Online
DOI: 10.1039/C5RA19343E

acceleration of the PbI_2 precursor film crystallization and slower PbI_2 crystallization process will result in tree fork shaped film. Our hypothesis is that uniform PbI_2 films would be obtained at the condition that the solvent in PbI_2 solution exhaust quickly and the PbI_2 crystallization process proceed quickly. As shown in Figure 2a, when applied an nitrogen flow during spin-coating process instead of increase the spin coating speed to increase PbI_2 recrystallization speed, PbI_2 film uniformity is improved under 3000 rpm (Figure 2d) and further improved under 5000 rpm with the thickness about 150~200 nm (Figure 2e).

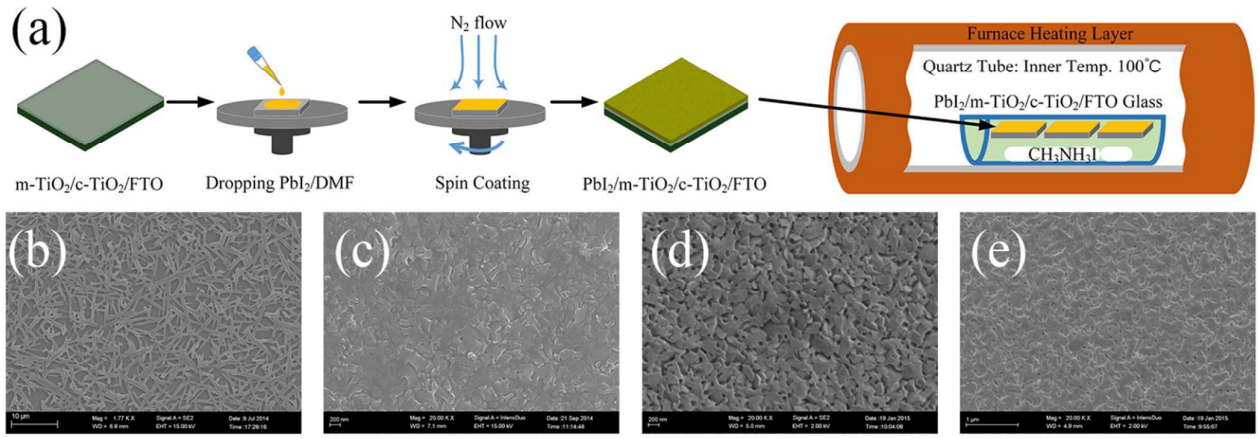

Fig. 2 (a) Schematic of optimized PbI_2 precursor films procedures and configuration of the subsequent HPCVD perovskite synthesis. Optimization of PbI_2 precursor films with spin coating process: top view SEM images of PbI_2 films spun coated at (b) 3000 rpm and (c) 5000 rpm in a spin coater with the cover closed; top view SEM images PbI_2 films spun coated at (d) 3000 rpm and (e) 5000 rpm with the cover open and a nitrogen flow added during the rotating of the substrates. The pressure of the nitrogen flow is 0.5 bar.

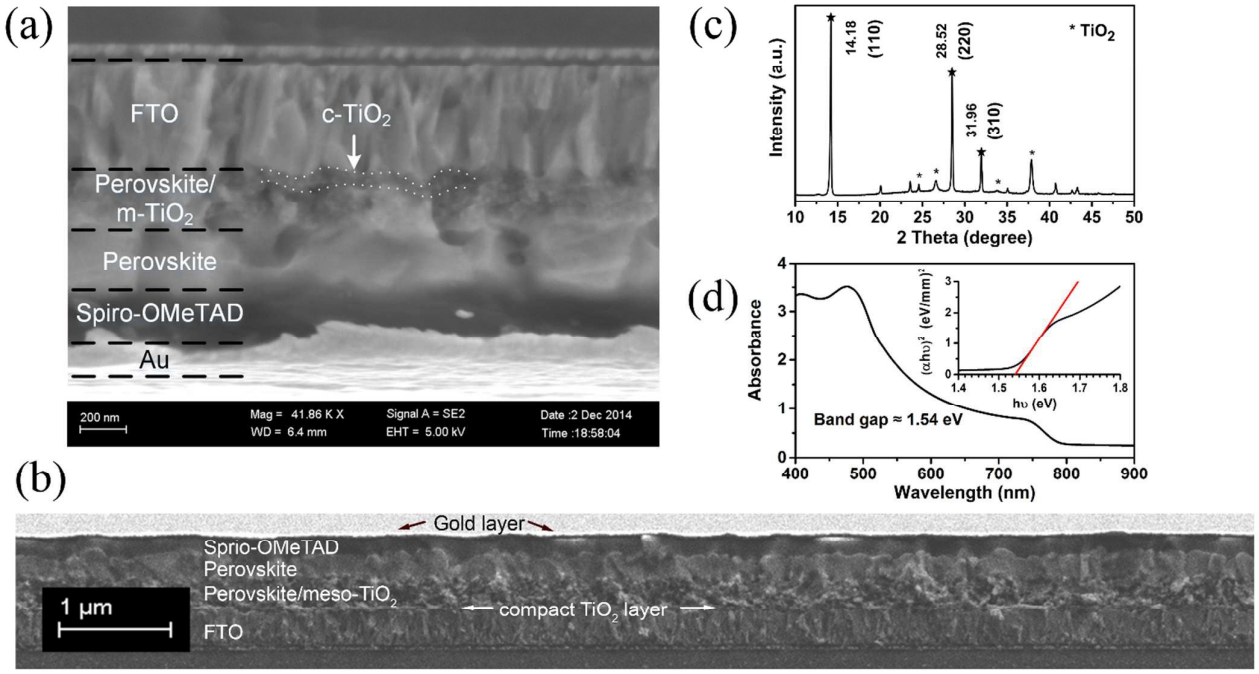

Fig. 3 Cross-sectional SEM images under of completed solar cells constructed from a HPCVD $CH_3NH_3PbI_3$ film with a thickness about 200 nm. (b) Cross-sectional SEM images under lower magnification of completed solar cells constructed from a HPCVD perovskite film. (c) XRD spectrum of the film after post thermal annealing and (d) absorbance spectrum of the film with derived bandgap of 1.54 eV.

Based on the optimized HPCVD method, high performance $CH_3NH_3PbI_3$ solar cells were fabricated. Detailed information of the fabrication process is described in supplementary information. As shown in Figure 3a, cross section of the perovskite solar cell was characterized by SEM. Uniform 200-nm-thick $CH_3NH_3PbI_3$ film was laminated between the spiro-OMeTAD (organic hole transport material) layer and the TiO_2 (electron transport material) layer. A cross-sectional SEM image of the whole perovskite solar cell with vision field longer than 10 μm was shown in Figure 3b, demonstrating

View Article Online
DOI: 10.1039/C5RA19343E

effectiveness of the HPCVD method to synthesize perovskite films. X-Ray Diffraction (XRD) spectrum of the $CH_3NH_3PbI_3$ film was shown in Figure 3c. Strong peaks in the XRD chart at 14.18°, 28.52°, 31.96°, which were corresponding to (110), (220), (310) miller indices of $CH_3NH_3PbI_3$ perovskite crystal, respectively, indicating the tetragonal crystal structure of perovskite. The absence of the PbI_2 charecteristic peak at 12.65°, demonstrates the full reaction between the two precursors in the HPCVD process. From the absorbance spectrum of the $CH_3NH_3PbI_3$ film, as shown in Figure 3d, bandgap of the perovskite material can be derived as 1.54 eV, in agreement with previous publications [38, 39].

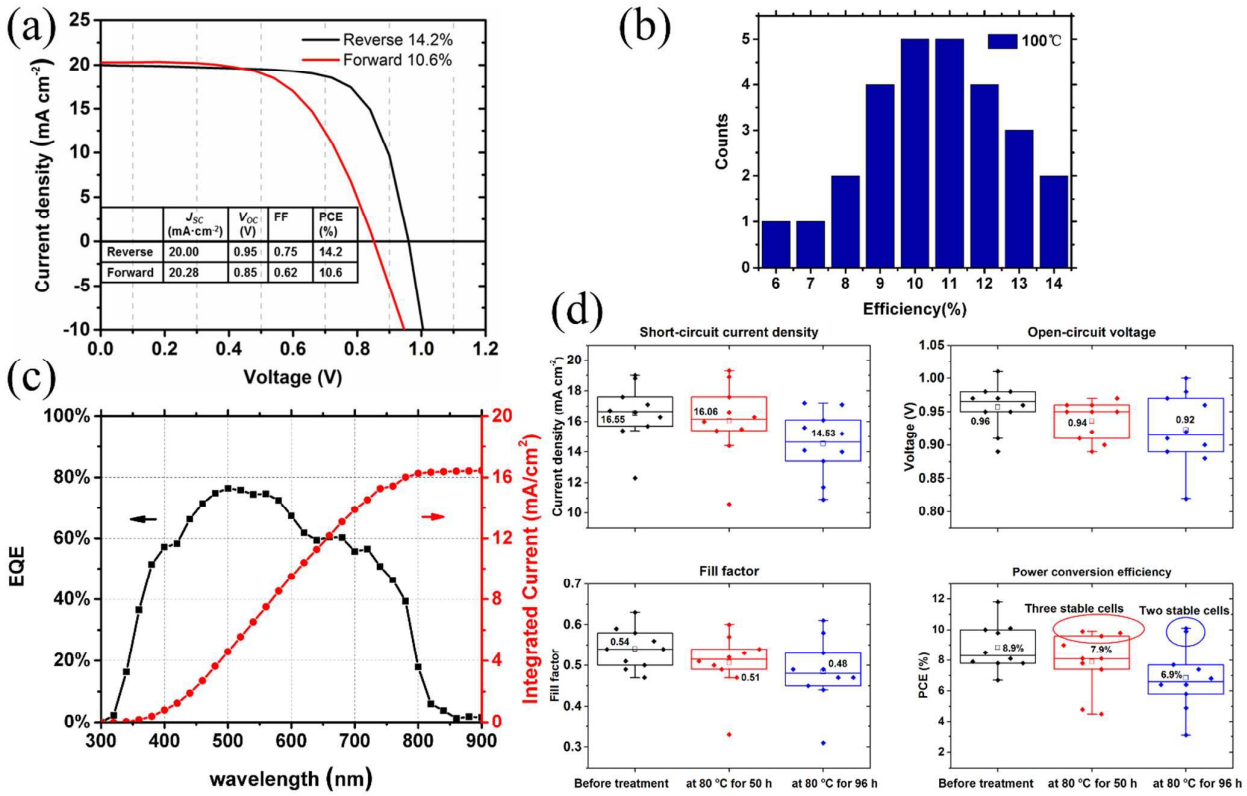

Fig. 4 (a) Current density-voltage curves of HPCVD $CH_3NH_3PbI_3$ solar cell measured under simulated AM 1.5 sunlight of 100mW cm^{-2} irradiance. (b) External quantum efficiency (EQE) spectrum of this device with integrated current density of 16.5 mA cm^{-2}. (c) Statistics of the efficiencies of 27 $CH_3NH_3PbI_3$ solar cells fabricated by the HPCVD method. Efficiencies of 17 devices are over 10%. (d) Performance of ten HPCVD solar cells were characterized after a treatment at 80 °C for 50 h and 96 h. Average PCE decreased from 8.9% to 7.9% and 6.9% after 50 h and 96 h heat treatment, respectively. Detailed information is shown in Table 1 and Table S1.

As show in Figure 4a, the best device by HPCVD display great performance, with reverse scan: J_{SC} = 20.00 mA cm^{-2}, V_{OC} = 0.95 V, fill factor (FF) = 75%, PCE = 14.2%; forward scan: J_{SC} = 20.28 mA cm^{-2}, V_{OC} = 0.85 V, fill factor (FF) = 62%, PCE = 10.6%. In general, 27 devices exhibit reversing scan PCE from 6.2% to 14.2% with a mean value of 11.1%, as shown in Figure 4b. External quantum efficiency (EQE) spectrum of the solar cell is shown in Figure 4c. By integrating the EQE spectrum value with the AM 1.5G solar photon flux between 300 nm and 900 nm, short circuit current density of 16.5 mA cm^{-2} can be derived, which is lower than J_{SC} from the *J-V* scanning and probably due to the interface defects of the TiO_2 layer reported in previous publications [18].

Table 1. Performance parameters of ten HPCVD solar cells before and after heat treatment at 80 °C for 50 h and 96 h.

	Avg. J_{SC} (mA cm^{-2})	Avg. V_{OC} (V)	Avg. FF	Avg. PCE (%)
Before heat treatment	16.55	0.96	0.54	8.9
After heated at 80 °C for 50 h	16.06	0.94	0.51	7.9
After heated at 80 °C for 96 h	14.53	0.92	0.48	6.9

Detailed information is shown in Table S1.

Finally, long term stability of solar cells by HPCVD were characterized in a controlled harsh environment (facilities shown in Figure S1) by heating ten solar cells at 80 °C for 50 hours and 96 hours, continuously. As shown in Figure 4d, the average PCE of the ten solar cells decayed gradually when the duration of the treatment increased, which is shown in Table

View Article Online
DOI: 10.1039/C5RA19343E

1. Detailed information of these solar cells is shown in Table S1. The average PCE of the ten solar cells decreased from 8.9% to 7.9% and 6.9% after 50 h and 96 h treatment, still maintaining 78% of their initial efficiencies. Meanwhile, among the ten solar cells, PCEs of two cells remained stable after 96 h harsh treatment as shown in Table S1. Perovskite solar cells whose organic hole transport material was poly(3-hexylthiophene) (P3HT) mixed with carbon nanotubes and polymethyl methacrylate (PMMA), showing stability at 80 °C for 96 hours with about 10% PCE decaying were reported, however, solar cells using Li-TSFI doped spiro-OMeTAD as hole transport material in the same reference failed after the same heat treatment [40]. Still, the HPCVD perovskite solar cells demonstrated relative high stability compared with previously perovskite solar cells, efficiency of which decreased rapidly when stored in nitrogen atmosphere [17].

Conclusions

In summary, high quality perovskite ($CH_3NH_3PbI_3$) films were synthesized trough a novel hybrid physical-chemical vapor deposition method for high performance solar cells. Due to the vacuum environment and isothermal environment, high quality and uniform $CH_3NH_3PbI_3$ films were obtained with grain sizes up to 800 nm and surface roughness around RMS 17.4 nm. Combined with optimized spin coating process for PbI_2 precursor film, a high-performance $CH_3NH_3PbI_3$ solar cell achieved high power conversion efficiency up to 14.2%. After treated in a controllable harsh environment (80 °C for 96 hours), a typical solar cell could still maintained decently high efficiency, demonstrating that the HPCVD method was effective and stable. In our further researches, more parameters of this HPCVD method and thermal annealing treatment will be modified to fabricate solar cells with better efficiency and stability. In future, the HPCVD perovskite solar cell could have great potential to be mass produced in low cost and large-scale applications.

Acknowledgements

This work was financially supported by the International Science and Technology Cooperation Program of Ministry of Science and Technology of the People's Republic of China (Grant No. 2013DFA51800).

Notes and references

1. M. A. Green, A. Ho-Baillie and H. J. Snaith, *Nature Photonics*, 2014, **8**, 506-514.
2. P. Gao, M. Gratzel and M. K. Nazeeruddin, *Energy & Environmental Science*, 2014, **7**, 2448-2463.
3. A. Kojima, K. Teshima, Y. Shirai and T. Miyasaka, *Journal of the American Chemical Society*, 2009, **131**, 6050-6051.
4. W. S. Yang, J. H. Noh, N. J. Jeon, Y. C. Kim, S. Ryu, J. Seo and S. I. Seok, *Science*, 2015, **348**, 1234-1237.
5. J. Yang, F. Luo, T. S. Kao, X. Li, G. W. Ho, J. Teng, X. Luo and M. Hong, *Light: Science & Applications*, 2014, **3**, e185.
6. C. F. Guo, T. Sun, F. Cao, Q. Liu and Z. Ren, *Light: Science & Applications*, 2014, **3**, e161.
7. M. Memarian and G. V. Eleftheriades, *Light: Science & Applications*, 2013, **2**, e114.
8. H. S. Kim, C. R. Lee, J. H. Im, K. B. Lee, T. Moehl, A. Marchioro, S. J. Moon, R. Humphry-Baker, J. H. Yum, J. E. Moser, M. Gratzel and N. G. Park, *Scientific reports*, 2012, **2**, 591.
9. J. Burschka, N. Pellet, S. J. Moon, R. Humphry-Baker, P. Gao, M. K. Nazeeruddin and M. Gratzel, *Nature*, 2013, **499**, 316-319.
10. N. J. Jeon, J. H. Noh, W. S. Yang, Y. C. Kim, S. Ryu, J. Seo and S. I. Seok, *Nature*, 2015, **517**, 476-480.
11. N. J. Jeon, J. H. Noh, Y. C. Kim, W. S. Yang, S. Ryu and S. I. Seok, *Nature materials*, 2014, **13**, 897-903.
12. P. Umari, E. Mosconi and F. De Angelis, *Scientific reports*, 2014, **4**, 4467.
13. G. Xing, N. Mathews, S. Sun, S. S. Lim, Y. M. Lam, M. Gratzel, S. Mhaisalkar and T. C. Sum, *Science*, 2013, **342**, 344-347.
14. S. D. Stranks, G. E. Eperon, G. Grancini, C. Menelaou, M. J. Alcocer, T. Leijtens, L. M. Herz, A. Petrozza and H. J. Snaith, *Science*, 2013, **342**, 341-344.
15. D. Shi, V. Adinolfi, R. Comin, M. Yuan, E. Alarousu, A. Buin, Y. Chen, S. Hoogland, A. Rothenberger, K. Katsiev, Y. Losovyj, X. Zhang, P. A. Dowben, O. F. Mohammed, E. H. Sargent and O. M. Bakr, *Science*, 2015, **347**, 519-522.
16. M. Liu, M. B. Johnston and H. J. Snaith, *Nature*, 2013, **501**, 395-398.
17. H. Zhou, Q. Chen, G. Li, S. Luo, T. B. Song, H. S. Duan, Z. Hong, J. You, Y. Liu and Y. Yang, *Science*, 2014, **345**, 542-546.
18. Q. Chen, H. Zhou, Z. Hong, S. Luo, H. S. Duan, H. H. Wang, Y. Liu, G. Li and Y. Yang, *Journal of the American Chemical Society*, 2014, **136**, 622-625.
19. M. Saba, M. Cadelano, D. Marongiu, F. Chen, V. Sarritzu, N. Sestu, C. Figus, M. Aresti, R. Piras, A. G. Lehmann, C. Cannas, A. Musinu, F. Quochi, A. Mura and G. Bongiovanni, *Nature communications*, 2014, **5**, 5049.
20. L. Wang, C. McCleese, A. Kovalsky, Y. Zhao and C. Burda, *Journal of the American Chemical Society*, 2014, **136**, 12205-12208.
21. V. W. Bergmann, S. A. Weber, F. Javier Ramos, M. K. Nazeeruddin, M. Gratzel, D. Li, A. L. Domanski, I. Lieberwirth, S. Ahmad and R. Berger, *Nature communications*, 2014, **5**, 5001.
22. E. Edri, S. Kirmayer, S. Mukhopadhyay, K. Gartsman, G. Hodes and D. Cahen, *Nature communications*, 2014, **5**, 3461.
23. J. Shi, J. Dong, S. Lv, Y. Xu, L. Zhu, J. Xiao, X. Xu, H. Wu, D. Li, Y. Luo and Q. Meng, *Applied Physics Letters*, 2014, **104**, 063901.
24. J. Wei, Y. Zhao, H. Li, G. Li, J. Pan, D. Xu, Q. Zhao and D. Yu, *The Journal of Physical Chemistry Letters*, 2014, **5**, 3937-3945.
25. C. Wehrenfennig, M. Liu, H. J. Snaith, M. B. Johnston and L. M. Herz, *Energy & Environmental Science*, 2014, **7**, 2269.
26. C. Wehrenfennig, G. E. Eperon, M. B. Johnston, H. J. Snaith and L. M. Herz, *Advanced materials*, 2014, **26**, 1584-1589.
27. F. Huang, Y. Dkhissi, W. Huang, M. Xiao, I. Benesperi, S. Rubanov, Y. Zhu, X. Lin, L. Jiang, Y. Zhou, A. Gray-Weale, J. Etheridge, C. R. McNeill, R. A. Caruso, U. Bach, L. Spiccia and Y.-B. Cheng, *Nano Energy*, 2014, **10**, 10-18.
28. Y. Dkhissi, F. Huang, S. Rubanov, M. Xiao, U. Bach, L. Spiccia, R. A. Caruso and Y.-B. Cheng, *Journal of Power Sources*, 2015, **278**, 325-331.
29. J. You, Y. Yang, Z. Hong, T.-B. Song, L. Meng, Y. Liu, C. Jiang, H. Zhou, W.-H. Chang, G. Li and Y. Yang, *Applied Physics Letters*, 2014, **105**, 183902.
30. B.-S. Kim, T.-M. Kim, M.-S. Choi, H.-S. Shim and J.-J. Kim, *Organic Electronics*, 2015, **17**, 102-106.
31. S. T. Ha, X. F. Liu, Q. Zhang, D. Giovanni, T. C. Sum and Q. H. Xiong, *Advanced Optical Materials*, 2014, **2**, 838-844.
32. D. J. Lewis and P. O'Brien, *Chemical communications*, 2014, **50**, 6319-6321.

View Article Online
DOI: 10.1039/C5RA19343E

33. M. R. Leyden, L. K. Ono, S. R. Raga, Y. Kato, S. H. Wang and Y. B. Qi, *Journal of Materials Chemistry A*, 2014, **2**, 18742-18745.
34. P. Luo, Z. Liu, W. Xia, C. Yuan, J. Cheng and Y. Lu, *ACS applied materials & interfaces*, 2015, **7**, 2708-2714.
35. W.-J. Yin, J.-H. Yang, J. Kang, Y. Yan and S.-H. Wei, *J. Mater. Chem. A*, 2015, **3**, 8926-8942.
36. Y. Peng, G. Jing and T. Cui, *J. Mater. Chem. A*, 2015, **3**, 12436-12442.
37. Y. Peng, G. Jing and T. Cui, in *MRS Proceedings*, Cambridge Univ Press, 2015, pp. mrss15-2135352.
38. G. Niu, X. Guo and L. Wang, *J. Mater. Chem. A*, 2015, **3**, 8970-8980.
39. W. Nie, H. Tsai, R. Asadpour, J. C. Blancon, A. J. Neukirch, G. Gupta, J. J. Crochet, M. Chhowalla, S. Tretiak, M. A. Alam, H. L. Wang and A. D. Mohite, *Science*, 2015, **347**, 522-525.
40. S. N. Habisreutinger, T. Leijtens, G. E. Eperon, S. D. Stranks, R. J. Nicholas and H. J. Snaith, *Nano letters*, 2014, **14**, 5561-5568.